Chapter 6 Top Quark Physics

1 Introduction

The linear collider, operating near the $t\bar{t}$ production threshold and at higher energies, can carry out a comprehensive program of top quark physics. Measurements at the threshold include the determination of the top quark mass, m_t, and width, Γ_t, as well as the top quark Yukawa coupling, g_{ttH}. The quantities m_t and g_{ttH} can also be measured at higher energies, together with the couplings of the top quark to the electroweak gauge bosons. In this chapter we present a brief summary of our current understanding of top quark physics at a linear collider.

The top is unique among the quarks in that it decays before nonperturbative strong interaction effects can influence it. Its large mass gives it stronger coupling to many proposed new physics effects that try to explain electroweak symmetry breaking and/or the origin of particle masses. Thus, precise measurement of the parameters of the top quark would provide important insights into physics beyond the Standard Model.

2 Physics in the threshold region

2.1 Introduction

One of the primary goals of a high-energy e^+e^- linear collider is the study of sharp features in the cross section for e^+e^- annihilation to hadrons. The $t\bar{t}$ threshold is an excellent example of such a structure. The cross section for $e^+e^- \to t\bar{t}$ is expected to rise by an order of magnitude with only a 5 GeV change in center-of-mass energy around 350 GeV. Careful study of this $t\bar{t}$ threshold structure can precisely measure many parameters of the top quark, including its mass and width, and the top quark Yukawa coupling. In this section we briefly summarize the current status of $t\bar{t}$ threshold studies. More comprehensive discussions can be found in [1–3].

2.2 QCD dynamics and cross section

It is well known that, because of the large top quark width ($\Gamma_t \approx 1.4\,\mathrm{GeV} \gg \Lambda_{QCD}$), a top-antitop pair cannot form narrow toponium resonances. Instead, the cross section is expected to have a smooth line-shape showing only a moderate $1S$ peak. The dynamics of the top quark in the threshold region is described by perturbative QCD. The top quark width serves as an infrared cutoff. As a result, nonperturbative QCD effects (as measured, for example, by the influence of the gluon

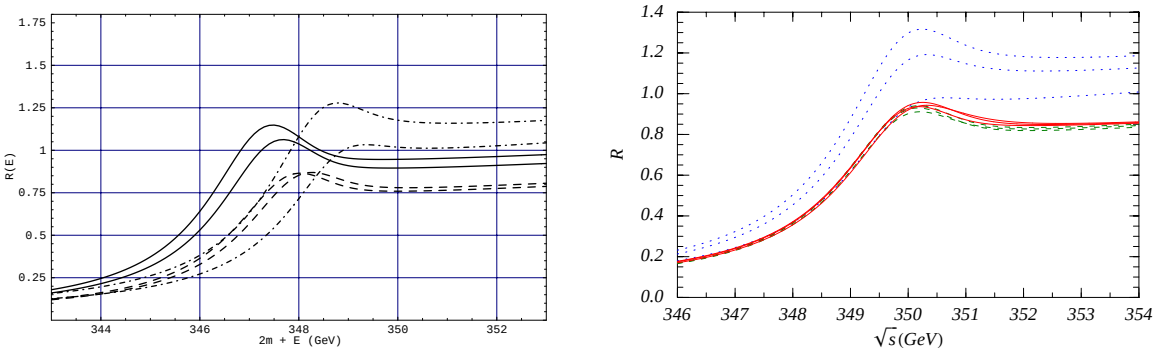

Figure 6.1: The normalized cross section $R_t = \sigma(e^+e^- \to t\bar{t})/\sigma(e^+e^- \to \mu^+\mu^-)$ as a function of $\sqrt{s}$, computed in QCD perturbation theory at various levels. These are theoretical curves that do not include initial state radiation, beamstrahlung, or beam energy spread. (**Left:**) The normalized cross section computed with the pole mass $m_t^{\rm pole} = 175$ GeV, at LO (dashed-dotted lines), NLO (dashed lines), and NNLO (solid lines). Each pair of the curves corresponds to the two different soft normalization scales $\mu = 30$ GeV (upper curve) and $\mu = 60$ GeV (lower curve). (**Right:**) The normalized cross section computed with the $1S$ mass $m_t^{1S} = 175$ GeV, at LL order (dotted), NLL order (dashed) and NNLL order in QCD (solid). The calculation includes the summation of logarithms of the top quark velocity, and at each order curves are shown for $\nu = 0.15, 0.2, 0.4$, where ν is the so-called subtraction velocity.

condensate) are small [4], allowing us, in principle at least, to calculate the cross section from QCD with high accuracy.

The convergence of QCD perturbation theory in the threshold region depends on the quark mass definition used. The simplest definition of m_t is the position of the pole in the top quark propagator. This 'pole mass' is similar to the kinematic mass observed in top quark pair production above threshold, and similar to the mass definition used by the CDF and DØ experiments in the original papers on the top quark discovery [5,6]. Unfortunately, with this choice of the mass definition, the NNLO corrections are uncomfortably large [1] and shift the $1S$ peak by about 0.5 GeV, spoiling the possibility to extract the top quark mass with high accuracy. The threshold cross sections computed at successive order in QCD are shown in the left-hand graph in Fig. 6.1. The instability of this perturbation series is caused by the fact that the pole mass has a renormalon ambiguity, that is, it obtains an additive correction from nonperturbative QCD effects.

To remove this difficulty, one can use a different mass definition that refers only to short-distance QCD physics. For example, a possible definition of the mass, called the $1S$ mass, is one-half of the mass of the lowest toponium bound state computed in the hypothetical limit of zero top quark width [7]. Three other mass definitions have been considered in the literature. The $\overline{\rm PS}$ mass [8] is defined via the top quark self-energy. The LS ('low scale') mass is given in terms of perturbative evaluations

of matrix elements of operators in the heavy quark effective theory that describe the difference between the pole mass and a fictitious T meson mass [9]. Finally, the PS ('potential-subtracted') mass is defined by

$$m_t^{PS}(\mu) = m_t^{\rm pole} + \frac{1}{2}\int\limits_{|k|<\mu} \frac{d^3k}{(2\pi)^3} V_C(k) = m_t^{\rm pole} - \frac{4}{3}\frac{\alpha_s}{\pi}\mu + ... \qquad (6.1)$$

where μ is the soft renormalization scale. All of these mass definitions, collectively called 'threshold masses' have the property that they are free of the $\mathcal{O}(\Lambda_{QCD})$ renormalon ambiguity [10,11]. These masses also have the property that they are connected to the $\overline{MS}$ top quark mass by a convergent QCD perturbation series.

The position of the $1S$ peak becomes much more stable at higher orders of QCD if threshold masses are used. The shifts from order to order are less than 100 MeV. However, a large theoretical normalization uncertainty of about 10% remains. The normalization uncertainty can be reduced to a few percent by resumming terms logarithmic in the top velocity. The convergence for the $1S$ mass definition is shown in the right-hand graph of Fig. 6.1 [12]. Simultaneous accurate measurements of the top mass and other quantities thus appear feasible, as discussed further below.

2.3 Top width

The scan of the $t\bar{t}$ threshold will allow a direct measurement of the top quark width, Γ_t. The cross section at the $1S$ quarkonium bound state energy is proportional to $1/\Gamma_t$. Realistic studies, which include initial state radiation and other effects, show that Γ_t can be measured with an experimental precision of a few percent [2], now that higher-order QCD corrections appear to be under control [12].

Γ_t can also be measured using the forward-backward asymmetry [13]. The $t\bar{t}$ vector coupling to γ and Z produces mainly S-wave states, while the axial-vector coupling from the $Zt\bar{t}$ vertex produces $t\bar{t}$ in a P state. The top quark width causes the S and P states to overlap and allows these states to interfere in the final angular distribution. This produces a forward-backward asymmetry. Since the top quark width controls the amount of S-P overlap, the asymmetry is sensitive to Γ_t. Realistic studies are needed to better quantify the experimental sensitivity.

2.4 Top quark Yukawa coupling

In addition to the QCD potential, the $t\bar{t}$ pair interacts via a Yukawa potential associated with Higgs boson exchange

$$V_{tth} = -\frac{g_{tth}^2}{4\pi}\,\frac{e^{-m_h r}}{r}, \qquad (6.2)$$

where m_h is the Higgs boson mass and g_{tth} is the Yukawa coupling. Therefore, top threshold measurements can also be used to determine g_{tth} if the Higgs boson is light.

A SM Higgs boson with a mass of 115 GeV enhances the normalization of the cross section by 5–8% at energies near the threshold. The theoretical uncertainty of the cross section in this region is 2–3% when the summation of logarithms of the top quark velocity is taken into account [12]. A precision measurement of the $t\bar{t}$ threshold cross section thus will be sensitive to the top Yukawa coupling. If we fix all other parameters and assume $m_h = 115\,\mathrm{GeV}$, then varying the SM Yukawa coupling by $\pm 14\%$ gives a $\pm 2\%$ variation in the normalization of the cross section near the $1S$ peak [14]. For larger values of m_h, the sensitivity to g_{tth} is expected to decrease. Again, realistic experimental studies that make use of recent theoretical advances in understanding the threshold cross section are needed.

2.5 Experimental issues

The experimental situation of the $t\bar{t}$ threshold is fairly well understood, and there has not been much progress since the experimental methods were reviewed at the 1999 Sitges meeting [15]. It is expected that the top mass can be measured with a statistical uncertainty of 40 MeV in a modest scan of 10 fb^{-1}, a small fraction of a year at typical design luminosities. A longer scan of about 100 fb^{-1} can determine the top width to 2%. A key experimental issue for the threshold study is the measurement of the $\mathrm{d}\mathcal{L}/\mathrm{dE}$ spectrum, but many complementary methods have been proposed. The issues are similar to and less severe than the measurement of the $\mathrm{d}\mathcal{L}/\mathrm{dE}$ spectrum needed for a precision W mass measurement from the W^+W^- threshold, discussed in Chapter 8, Section 2. The limitations are likely to come from the uncertainty in machine-generated backgrounds and from the theoretical understanding of the Bhabha cross section. The impact of a precision top quark mass measurement can be seen in [16] and [17], which show how the current knowledge of the top mass and precision electroweak measurements limit the range of the Higgs mass and anomalous W and Z couplings caused by new physics.

3 Physics above the top threshold

3.1 Determination of the top quark–Higgs Yukawa coupling

3.1.1 Introduction

If there is a light Higgs boson, this particle is likely to be discovered at the Tevatron or the LHC. The role of a high-energy e^+e^- linear collider is then to test the connection of this particle to the physics of mass generation by accurately measuring its mass, width, and couplings to bosons and fermions. The top quark provides a unique opportunity to measure the Higgs Yukawa coupling to fermions through the process $e^+e^- \to t\bar{t}h$. For a light Higgs boson, the Higgs decays dominantly to $b\bar{b}$. Assuming

BR($t \to Wb$) = 100%, this leads to multi-jet event topologies involving 4 b-jets in the final state. Therefore, one of the crucial experimental aspects will be flavor tagging.

3.1.2 Basic scenario

The rate for $e^+e^- \to t\bar{t}h$ has been calculated to $\mathcal{O}(\alpha_s)$ and is less than 1 fb at $\sqrt{s} = 500$ GeV. The total cross section decreases at low $\sqrt{s}$ because of limited phase space and approaches a constant at high $\sqrt{s}$. The maximum of the cross section (for a 100–150 GeV Higgs boson) occurs around $\sqrt{s} \simeq 700$–800 GeV.

Since the Yukawa coupling is determined from the cross section measurement, it is straightforward to estimate the statistical and some systematic uncertainties on g_{tth} for a selection with efficiency ϵ and purity ρ, with an integrated luminosity L:

$$\left(\frac{\Delta g_{tth}}{g_{tth}}\right)_{\rm stat} = \frac{1}{S_{\rm stat}(g^2_{tth})\sqrt{\epsilon\rho L}}, \tag{6.3}$$

$$\left(\frac{\Delta g_{tth}}{g_{tth}}\right)_{\rm syst} = \frac{1}{S_{\rm syst}(g^2_{tth})}\left[\frac{1-\rho}{\rho}\frac{\Delta\sigma_B^{\rm eff}}{\sigma_B^{\rm eff}} \oplus \frac{1}{\rho}\frac{\Delta L}{L} \oplus \frac{\Delta\epsilon}{\epsilon}\right], \tag{6.4}$$

where $(\Delta g_{tth}/g_{tth})_{\rm syst}$ accounts for the uncertainties in the effective background cross-section (after selection), the integrated luminosity and the selection signal efficiency. $S_{\rm stat}(g^2_{tth})$ and $S_{\rm syst}(g^2_{tth})$ are defined as:

$$S_{\rm stat}(g^2_{tth}) = \frac{1}{\sqrt{\sigma_{tth}}}\left|\frac{d\sigma_{tth}}{dg^2_{tth}}\right|, \quad S_{\rm syst}(g^2_{tth}) = \frac{1}{\sigma_{tth}}\left|\frac{d\sigma_{tth}}{dg^2_{tth}}\right|. \tag{6.5}$$

$S_{\rm stat}$ reaches a 'plateau' for $\sqrt{s} \geq 700$ GeV, whereas $S_{\rm syst}$ is essentially independent of $\sqrt{s}$. At $\sqrt{s} = 800$ GeV, $S_{\rm stat} \simeq 3.09$ fb$^{1/2}$ and $S_{\rm syst} \simeq 1.92$. Therefore, assuming $\epsilon = 5\%$ and $\rho = 50\%$, a statistical precision of around 6.5% could be achieved in g_{tth} for $\sqrt{s} \geq 700$ GeV and $L = 1000$ fb^{-1}. The case is considerably worse at $\sqrt{s} = 500$ GeV where $S_{\rm stat} = 0.9$ fb$^{1/2}$, leading to a statistical uncertainty of 22% on the Yukawa coupling measurement (with $\epsilon = 5\%$ and $\rho = 50\%$). The systematic uncertainty is dominated by the uncertainty in the background normalization, if one assumes that both the signal selection efficiency and integrated luminosity can be known at the 1% level or better [18].

3.1.3 Analysis

We consider the process $e^+e^- \to t\bar{t}h \to W^+W^-b\bar{b}b\bar{b}$ in both semileptonic and fully hadronic W decay channels. In spite of the apparently clean signature of both channels (≥ 6 jets in the final state, with ≥ 4 b-jets and multi-jet invariant mass constraints), the measurement has many difficulties. Among these are the tiny signal with backgrounds about 3 orders of magnitude larger, the limitations of jet-clustering

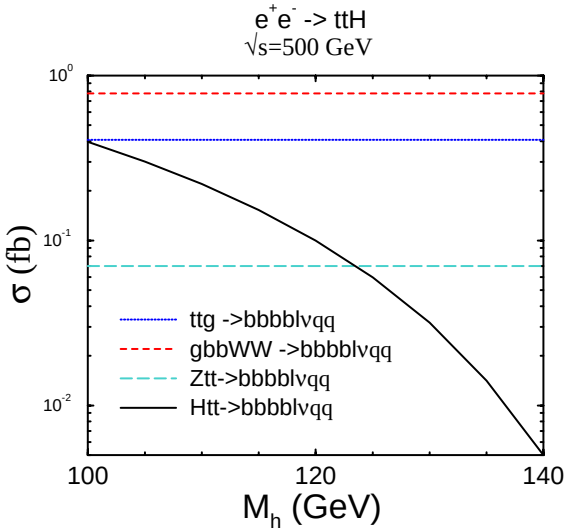

Figure 6.2: Parton level signal and backgrounds to $e^+e^- \to t\bar{t}h$ at $\sqrt{s} = 500$ GeV.

algorithms in properly reconstructing multi-jets in the final state, and the degradation of b-tagging performance due to hard gluon radiation and jet mixing.

The dominant electroweak background to the semi-leptonic decay is [18–20]:

$$e^+e^- \to t\bar{t}Z \to ZW^+W^-b\bar{b} \to b\bar{b}b\bar{b}\ell^\pm\nu q\bar{q}'.$$

The largest background is from radiative top quark decays:

$$e^+e^- \to t\bar{t} \to gW^+W^-b\bar{b} \to b\bar{b}b\bar{b}\ell^\pm\nu q\bar{q}'.$$

This background has been calculated at the parton level [20] and is shown in Fig. 6.2. Since the b jets resulting from the gluon splitting are logarithmically enhanced at low energy, cuts on the jet energy are effective at eliminating this background. A preliminary study of $e^+e^- \to t\bar{t}h$ at $\sqrt{s} = 500$ GeV included statistical, but not systematic errors and found that the top quark-Higgs Yukawa coupling could be measured with $\sim 21\%$ accuracy with perfect b-tagging and $L = 1000$ fb^{-1} [19].

The case for a 120 GeV Higgs boson and $\sqrt{s} = 800$ GeV with $L = 1000$ fb^{-1} has been considered in [18], with events processed through a simulation of a detector for TESLA. In this analysis, the b jets are defined as those four jets with the lowest probability to originate from the primary vertex. The analysis applies a standard preselection in order to remove as much background as possible while keeping a high efficiency for the signal. Then, in order to improve the statistical sensitivity further, a multivariate analysis using a Neural Network (NN) is performed. After preselection, the overall effective cross section for the background is 17.60 fb, while for the signal it is only 0.61 fb. This translates into such a poor sample purity ($\rho \sim 3.3\%$), that any uncertainty in the background normalization completely erases the significance in the

signal. After the NN analysis [18], the statistical error is reduced to 5.1%, and the systematic error to 3.8%, leading to an overall uncertainty of 6.3% for the Yukawa coupling measurement in the semi-leptonic channel. Combining this with the analysis for the hadronic channel gives a total uncertainty of 5.5%.

3.1.4 Conclusion

The reaction $e^+e^- \to t\bar{t}h$ allows a direct determination of the top quark-Higgs Yukawa coupling. For $m_h = 120$ GeV and $\mathcal{L} = 1000$ fb^{-1}, a total uncertainty of roughly 5.5% on the top-Higgs Yukawa coupling at $\sqrt{s} = 800$ GeV can be obtained. Preliminary studies show that the anticipated precision is about a factor of 4 worse at $\sqrt{s} = 500$ GeV. The dominant systematic uncertainty is from the overall background normalization, pointing to the importance of a complete $2 \to 8$ background calculation.

3.2 Top mass reconstruction

The top quark mass in e^+e^- collisions can not only be measured in a threshold scan, but also at center-of-mass energies above the $t\bar{t}$ threshold. A recent study [21] has shown that a statistical precision of 200 MeV or better may be reached for the top mass from a full kinematical reconstruction of $e^+e^- \to t\bar{t} \to W^+bW^-\bar{b} \to \ell^+\nu b\ell^-\bar{\nu}\bar{b}$ events. It should be noted that the mass measured from final-state shape variables is the pole mass, which is subject to a theoretical uncertainty of $\mathcal{O}(\Lambda_{QCD})$; this point was explained in Section 2.2. Here we give a brief status report of a new study that focuses on extracting the top quark mass from the the b-ℓ invariant mass distribution $d\sigma/dm_{b\ell}$, where ℓ is the lepton from the W decay, and the b-quark energy spectrum, $d\sigma/dE_b$.

The extraction of the top mass from final-state shape variables is best done using templates, using a method similar to that described in [22]. It depends crucially on the modeling of the multiparton radiation that is associated with the top production and decay stages. Standard Monte Carlo event generators simulate multiple emission in the soft or collinear approximation and leave empty regions of the phase space corresponding to hard and large-angle gluon radiation ("dead zones"), which can be populated using the exact matrix element ("matrix-element corrections"). Matrix-element corrections to top decays $t \to bW(g)$ [23] have been implemented in the most recent version of the HERWIG event generator, HERWIG 6.2 [24], which is used in the following. These corrections were found to have a significant effect on jet observables and on the top mass measurement at lepton and hadron colliders [23,25].

The $m_{b\ell}$ distribution, within the precision of the Monte Carlo integration, is independent of the hard-scattering process and of the center-of-mass energy. $m_{b\ell}$ is a Lorentz-invariant observable and is therefore insensitive to the boost from the top

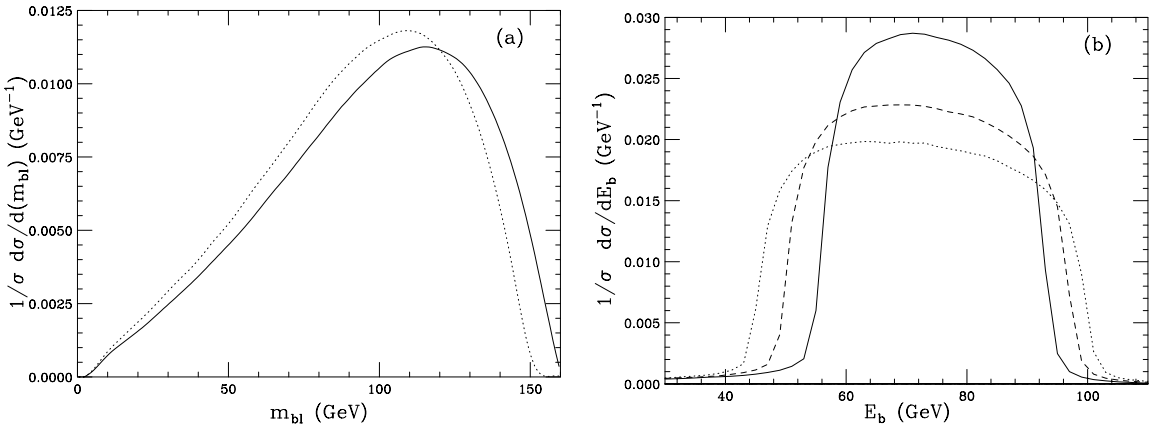

Figure 6.3: a) Invariant mass $m_{b\ell}$ distributions for $m_t = 171$ GeV (dotted line) and $m_t = 179$ GeV (solid line). b) b-quark energy distribution at $\sqrt{s} = 370$ GeV, for $m_t = 179$ GeV (solid), 175 GeV (dashed) and 171 GeV (dotted).

quark rest frame to the laboratory frame. In Fig. 6.3a we plot the $m_{b\ell}$ distribution for $m_t = 171$ GeV and 179 GeV. As m_t increases, the peak position of the $m_{b\ell}$ distribution is shifted towards larger values. The average value $\langle m_{b\ell} \rangle$ is proportional to the top quark mass. The best fit is:

$$\langle m_{b\ell} \rangle \ = \ 0.756\ m_t - 37.761\ \text{GeV},\ \epsilon = 0.002\ \text{GeV}, \tag{6.6}$$

where ϵ is the mean square deviation in the fit. Solving Eq. (6.6), one finds $\Delta m_t \approx 1.32\ \Delta\langle m_{b\ell} \rangle$, where $\Delta\langle m_{b\ell} \rangle$ is the uncertainty on the measurement of $\langle m_{b\ell} \rangle$. No detailed study of the precision that can be achieved with this method has been carried out yet.

In contrast to $m_{b\ell}$, the b-quark energy E_b is not a Lorentz-invariant observable. One therefore expects that the E_b distribution does depend on the boost from the top rest frame to the laboratory frame, and hence on the center-of-mass energy. Since the $t\bar{t}$ pair is produced almost at rest at the $t\bar{t}$ threshold, the dependence of E_b on the top mass is maximized in this region. The E_b distribution for $\sqrt{s} = 370$ GeV and several values of m_t is shown in Fig. 6.3b. For m_t approaching the threshold value of $\sqrt{s}/2$, the E_b distribution becomes very narrow. The half-maximum width σ_b therefore shows a strong dependence on the top mass. The best polynomial fit to express σ_b in terms of m_t for $\sqrt{s} = 370$ GeV is found to be:

$$\sigma_b = \ -0.081\ m_t^2 + 26.137\ m_t - 2048.968\ \text{GeV},\ \epsilon = 0.393\ \text{GeV}. \tag{6.7}$$

For a top quark mass in the range 171 GeV $\lesssim m_t \lesssim$ 179 GeV, the induced uncertainty on m_t is $\Delta m_t \approx 0.35 - 0.65\ \Delta\sigma_b$, where $\Delta\sigma_b$ is the uncertainty on the half-maximum width. E_b thus may be an interesting observable to reconstruct the top mass at energies slightly above the $t\bar{t}$ threshold. It is probably less useful at higher energies.

3.3 Anomalous couplings

At present, the couplings of the top quark to gluons and the electroweak gauge bosons are largely untested. A linear collider provides an ideal tool to probe the couplings of the top quark to the electroweak gauge bosons. It is important to note that the neutral electroweak couplings are accessible only at lepton colliders, because top quarks at hadron colliders are pair-produced via gluon exchange. Since the charged electroweak current is involved in the top decay, $t\overline{t}$ production in e^+e^- collisions is sensitive to both the neutral and charged gauge boson couplings of the top quark. Because the top quark width, Γ_t, is much larger than $\Lambda_{\rm QCD}$, the decay process is not influenced by fragmentation effects and decay products will provide useful information.

The most general $(\gamma,\, Z)t\overline{t}$ couplings can be written as [26,27]

$$\Gamma^{\mu}_{t\overline{t}\,\gamma,Z} = i\,e\,\left\{\gamma^{\mu}\,\left[F_{1V}^{\gamma,Z}\,+F_{1A}^{\gamma,Z}\,\gamma^5\right] + \frac{(\,p_t - p_{\overline{t}})^{\mu}}{2\,m_t}\,\left[F_{2V}^{\gamma,Z}\,+F_{2A}^{\gamma,Z}\,\gamma^5\right]\right\}\,, \tag{6.8}$$

where the only form factors different from zero in the SM are

$$F_{1V}^{\gamma} = \frac{2}{3}\,,\; F_{1V}^{Z} = \frac{1}{4\sin\theta_W\cos\theta_W}\,\left(1-\frac{8}{3}\sin^2\theta_W\right)\,,\; F_{1A}^{Z} = -\frac{1}{4\sin\theta_W\cos\theta_W}. \tag{6.9}$$

$(e/m_t)\cdot F_{2A}^{\gamma}$ is the CP-violating electric dipole moment (EDM) form factor of the top quark and $(e/m_t)\cdot F_{2A}^{Z}$ is the weak electric dipole moment (WDM). $(e/m_t)\cdot F_{2V}^{\gamma,Z}$ are the electric and weak magnetic dipole moments (MDM).

In the SM, the EDM and WDM terms violate CP and receive contributions only at the three-loop level and beyond. The CP-conserving form factors are zero at tree level but receive non-zero $\mathcal{O}(\alpha_s)$ QCD corrections.

The most general Wtb couplings can be parametrized in the form [27]

$$\Gamma^{\mu}_{tbW} = -\frac{g}{\sqrt{2}}\,V_{tb}\,\left\{\gamma^{\mu}\,\left[f_1^L\,P_L + f_1^R\,P_R\right] - \frac{i\,\sigma^{\mu\nu}}{M_W}\,(p_t-p_b)_{\nu}\,\left[f_2^L\,P_L + f_2^R\,P_R\right]\right\}\,, \tag{6.10}$$

where $P_{R,L} = (1\pm\gamma_5)/2$. In the limit $m_b\to 0$, f_1^R and f_2^L vanish. In the SM, at tree level, $f_1^L = 1$, and all other form factors are zero. Similarly, the $W\overline{t}\overline{b}$ vertex function can be parametrized in terms of form factors $\overline{f}_{1,2}^{L,R}$. If CP is conserved, $\overline{f}_{1,2}^{L,R} = f_{1,2}^{L,R}$.

In Table 6.1, we present the 1σ sensitivity limits for the real parts of the $(\gamma,\, Z)t\overline{t}$ form factors obtained from a recent analysis of the process $e^+e^-\to t\overline{t}\to \ell^{\pm}+$ jets at $\sqrt{s} = 500$ GeV. Only one coupling at a time is varied. Top quarks are selected and reconstructed, and b quarks are tagged using the LCD fast simulation package for the L detector configuration. The combined efficiency is 20%, and the purity after selection is 88%. To extract limits on $F_{1V}^{\gamma,Z}$ and $F_{1A}^{\gamma,Z}$, the angular distribution of the reconstructed top quark is used. $F_{1V}^{\gamma,Z}$ and $F_{2V}^{\gamma,Z}$ are derived from the left-right

Coupling	LO SM Value	$\mathcal{P}(e^-)$	$\int \mathcal{L}dt$ (fb^{-1})	1σ sensitivity
F_{1A}^{γ}	0	± 0.8	100	0.011
F_{1A}^{Z}	-0.6	-0.8	100	0.013
F_{1V}^{γ}	2/3	± 0.8	200	0.047
F_{1V}^{Z}	0.2	± 0.8	200	0.012
F_{2A}^{γ}	0	$+0.8$	100	0.014
F_{2A}^{Z}	0	$+0.8$	100	0.052
F_{2V}^{γ}	0	± 0.8	200	0.038
F_{2V}^{Z}	0	± 0.8	200	0.009

Table 6.1: The 1σ statistical uncertainties for the real parts of the $(\gamma, Z)t\bar{t}$ form factors obtained from an analysis of the process $e^+e^- \to t\bar{t} \to \ell^{\pm}+$ jets for $\sqrt{s} = 500$ GeV. Only one coupling at a time is varied.

polarization asymmetry, and $F_{2A}^{\gamma,Z}$ from the angular distribution of the reconstructed top quark and the decay angles of the t and $\bar{t}$.

The limits shown in Table 6.1 could be strengthened if positron beam polarization becomes available, mostly from the increased $t\bar{t}$ cross section. If $\mathcal{P}(e^+) = 0.5$, the $t\bar{t}$ cross section is about a factor 1.45 larger than that obtained with $\mathcal{P}(e^+) = 0$. This improves the bounds by up to 25%. Increasing the CM energy to $\sqrt{s} = 800$ GeV improves the limits by a factor 1.3–1.5 [28].

The decay form factor f_2^R, corresponding to a $(V + A)$ top decay, can be measured with a precision of about 0.01 for $\sqrt{s} = 500$ GeV and $\int \mathcal{L}dt = 500$ fb^{-1} if electron and positron beam polarization are available [27]. This quantity can also be measured at the LHC, though the expected limit is a factor three to eight weaker than the limit we project for a linear collider [29].

Many models predict anomalous top quark couplings. In technicolor models and other models with a strongly-coupled Higgs sector, the CP-conserving couplings may be induced at the 5–10% level [30–32]. In supersymmetric and multi-Higgs models, the CP-violating couplings $F_{2V,A}^{\gamma,Z}$ may be induced at the one-loop level, with predictions in the range $F_{2V,A}^{\gamma,Z} = \mathcal{O}(10^{-3} - 10^{-2})$ [17]. A measurement of the $(\gamma, Z)t\bar{t}$ couplings at a linear collider will thus be sensitive to interesting sources of non-SM physics.

3.4 QCD and electroweak radiative corrections

For $\sqrt{s} = 500$ GeV and an integrated luminosity of 500 fb^{-1}, the statistical error of the $e^+e^- \to t\bar{t} \to \ell\nu jj\bar{b}b$ cross section is well below 1%. In order to match this experimental accuracy with robust theoretical predictions, precision calculations beyond tree level are required. Such theoretical accuracy is needed both when top itself is the subject of study and when top is a background to other physics of interest.

QCD corrections can have important effects in top events. Jets from radiated gluons can be indistinguishable from quark jets, complicating identification of top quark events from the reconstruction of the top decay products. In addition, real emission may occur either in the top production or decay processes, so that radiated gluons may or may not themselves be products of the decay. Subsequent mass measurements can be degraded, not only from misidentification of jets but also from subtle effects such as jet broadening when gluons are emitted near other partons. Virtual corrections must also be included to predict correct overall rates.

Most calculations of QCD corrections in $e^+e^- \to t\overline{t}$ to date have been performed for on-shell top quarks. In this approximation, corrections to the production and decay processes can be computed separately. A calculation of the QCD corrections to the production process $e^+e^- \to t\overline{t}$, which includes real gluon emission from the t and $\overline{t}$ and virtual gluon exchange between the t and $\overline{t}$ has been presented in [33]. A discussion of the QCD corrections to the decay $t \to Wb$ can be found in [34]; QCD corrections are found to reduce the tree-level width of 1.55 GeV to $\Gamma_t^{\mathcal{O}(\alpha_s)} = 1.42$ GeV after all the known QCD and EW corrections are taken into account.

Because of the large width of the top quark and the fact that it does not hadronize before decaying [35], it is necessary to compute corrections to the entire production and decay process, including off-shell effects. In the soft gluon approximation, real gluon corrections for the process $e^+e^- \to t\overline{t} \to WWbb$ with the top allowed to be off-shell were calculated in [36]. Interference effects of gluons radiated in the production and decay stages were found to be sensitive to the top width Γ_t, with the effects being largest for gluon energies comparable to Γ_t. Similarly, real gluon radiation in top production and decay is sensitive to top width effects [37].

Since the process observed experimentally is

$$e^+e^- \to \; b\, W^+\, \overline{b}\, W^-\,, \tag{6.11}$$

it is desirable to take into account all Feynman diagrams that contribute to (6.11). This has not been done yet. At next-to-leading order, it is sufficient to take into account only the QCD corrections to the diagrams containing an intermediate top and antitop quark, as has been done in the computations discussed here. This approach uses the double pole approximation (DPA), in which only the double resonant terms (due to top and antitop propagators) are kept. Work done in this area follows closely the treatment of the W pair production process at LEP II [38].

Radiative corrections to $e^+e^- \to t\overline{t} \to bW^+\overline{b}W^-$ are usually split into two classes: corrections to particular subprocesses (production and decay), also called factorizable corrections, and corrections involving interference between these subprocesses (non-factorizable corrections). In most approaches, the factorizable corrections are computed using the on-shell approximation for the top quarks; either using the on-shell phase space, or making an on-shell projection from the exact phase space [39,40]. In the latter the on-shell projection restricts the effect of the off-shell particles to the

$2E_{beam}$	360 GeV	500 GeV	1000 GeV
σ_0	0.386 pb	0.565 pb	0.172 pb
$\sigma_1^{on-shell}$	0.737 pb	0.666 pb	0.186 pb
σ_1^{DPA}	0.644 pb	0.652 pb	0.191 pb

Table 6.2: Cross sections (tree level, on-shell NLO and DPA NLO) for top production and decay at a linear collider [41]; results do not include ISR, beamstrahlung or beam energy spread.

interference terms. These interference terms are computed in DPA, for virtual as well as for real gluons. As a consequence, interference terms do not contribute to the total cross section.

In [41], a different approach is used. Instead of starting with the on-shell computation and adding the nonfactorizable corrections, the starting point is the exact amplitudes for the off-shell process from which terms that are not doubly resonant are dropped. Also, the real gluon contributions are treated exactly (as in [37]); as a consequence, the cancellation between virtual gluon and real gluon interference is no longer complete. Table 6.2 summarizes the total cross section results. The QCD corrections are found to increase the $t\bar{t}$ production cross section by up to a factor two near the threshold, and by about 11–13% in the continuum.

Electroweak $\mathcal{O}(\alpha)$ corrections for top processes at linear colliders have also been computed so far only to on-shell $t\bar{t}$ production and top decay. The electroweak $\mathcal{O}(\alpha)$ corrections can be naturally subdivided into two gauge-invariant subclasses, QED and weak corrections. The QED corrections depend on the cuts imposed on the photon phase space and thus on the experimental setup. As discussed in [42], initial-state $\mathcal{O}(\alpha)$ QED corrections can significantly reduce the cross section because of large logarithms of the form $\alpha/\pi \ln(s/m_e^2)$ with $s \gg m_e^2$. These terms arise when photons are radiated off in the direction of the incoming electrons. Thus, the inclusion of higher-order initial-state radiation (ISR) has to be considered. The leading-log initial-state QED corrections are universal and can be calculated using the so-called structure function approach [43].

The model-dependent contributions to corrections to top pair production are contained in the weak corrections. The numerical impact of the weak one-loop corrections is discussed in detail in [42]. Close to the $t\bar{t}$ threshold, the weak corrections to $\sigma_{t\bar{t}}$ are found to be quite sensitive to the Higgs boson mass. An updated analysis of the weak corrections to $\sigma_{t\bar{t}}$, using the current value of the top-quark mass, is presented in [44]. The weak corrections are found to reduce the Born cross section (expressed in terms of G_μ) near threshold by about 7%, which is mainly due to the box diagrams.

The complete electroweak $\mathcal{O}(\alpha)$ corrections to Γ_t are calculated in [45]. When using G_μ and M_W to parametrize the lowest-order top decay width, the electroweak

Observable	Precision	$\int \mathcal{L} dt$ (fb^{-1})	$\sqrt{s}$ (GeV)	Comment
m_t	< 100 MeV	10	350	theory dominated
m_t	200 MeV	50	500	not fully explored
Γ_t	$\mathcal{O}(30$ MeV)	100	350	not fully explored
g_{tth}	$\mathcal{O}(10\%)$	100	350	need realistic study
g_{tth}	21%	1000	500	stat. uncert. only
g_{tth}	5.5%	1000	800	need improved bgd. estimate
$F_{iV,A}^{\gamma,Z}$, f_2^R	$0.01 - 0.2$	500	500	polarized beams essential

Table 6.3: Summary of top quark-related measurements at a linear e^+e^- collider.

corrections amount to typically 1-2 % with no significant dependence on m_h.

Ultimately it will be necessary to combine the QCD and electroweak corrections to top processes. This has been done for $e^+e^- \to t\bar{t}$ in [46], and work is in progress to combine both types of correction for the entire production and decay process [47].

4 Conclusions

Remarkable progress has been made in the last two years in our theoretical understanding of $t\bar{t}$ production in e^+e^- collisions at the threshold. Problems associated with defining the top quark mass in a way that removes QCD ambiguities have been solved. The remaining theoretical uncertainties are sufficiently small to allow a simultaneous measurement of m_t (to 100 MeV), Γ_t (to a few percent) and g_{tth}. The top quark mass can also be measured with a precision of 200 MeV or better at higher energies, using a variety of kinematic variables. Not all interesting variables have been fully explored yet. An ideal process to determine the top quark Yukawa coupling at energies above the $t\bar{t}$ threshold is $t\bar{t}h$ production in e^+e^- collisions. However, to fully exploit this process, energies significantly larger than $\sqrt{s} = 500$ GeV are necessary. On the other hand, a center-of-mass energy of 500 GeV is sufficient to measure the top quark couplings to the electroweak gauge bosons with a precision of $\mathcal{O}(1 - 10\%)$. Polarized electron and positron beams are essential to disentangle the various couplings. We have summarized the estimated precision on the various quantities in Table 6.3. Finally, we have given a brief overview of the status of calculations of the QCD and electroweak corrections to $e^+e^- \to t\bar{t}$. The potential for precision studies of top quark physics at a linear collider requires a detailed understanding of these corrections.

References

[1] A. H. Hoang *et al.*, Eur. Phys. J. direct **C3**, 1 (2000).

[2] K. Fujii, T. Matsui and Y. Sumino, Phys. Rev. **D50**, 4341 (1994).

[3] S. Kuhlman *et al.*, hep-ex/9605011; J. Bagger *et al.*, hep-ex/0007022; E. Accomando *et al.*, Phys. Rep. **299**, 1 (1998).

[4] V. S. Fadin and O. Yakovlev, Sov. J. Nucl. Phys. **53**, 688 (1991); Sov. J. Nucl. Phys. **53**, 1053 (1991); M. J. Strassler and M. E. Peskin, Phys. Rev. **D43**, 1500 (1991).

[5] F. Abe *et al.* [CDF Collaboration], Phys. Rev. Lett. **74**, 2626 (1995) [hep-ex/9503002].

[6] S. Abachi *et al.* [DØ Collaboration], Phys. Rev. Lett. **74**, 2632 (1995) [hep-ex/9503003].

[7] A. Hoang and T. Teubner, Phys. Rev. **D60**, 114027 (1999).

[8] O. Yakovlev and S. Groote, Phys. Rev. D **63**, 074012 (2001) [hep-ph/0008156].

[9] I. I. Bigi *et al.*, Phys. Rev. **D56**, 4017 (1997).

[10] M. Beneke, Phys. Lett. **B434**, 115 (1998).

[11] A. H. Hoang *et al.*, Phys. Rev. **D59**, 114014 (1999); N. Uraltsev, in "Varenna 1997, Heavy flavor physics", hep-ph/9804275.

[12] A. Hoang *et al.*, Phys. Rev. Lett. **86**, 1951 (2001).

[13] H. Murayama and Y. Sumino, Phys. Rev. **D47**, 82 (1993).

[14] A. Hoang, A. Manohar, I. Stewart, and T. Teubner, in preparation.

[15] M. Martinez in *Physics and Experiments with Future Linear e^+e^- Colliders*, eds. E. Fernandez and A. Pacheco (1999) Barcelona and references therein.

[16] M. E. Peskin and J. D. Wells, hep-ph/0101342.

[17] M. Jeżabek, T. Nagano, and Y. Sumino, Phys. Rev. **D62**, 014034 (2000) and references therein.

[18] A. Juste and G. Merino, hep-ph/9910301.

[19] H. Baer, S. Dawson and L. Reina, Phys. Rev. **D61**, 013002 (2000).

[20] S. Moretti, hep-ph/9911501.

[21] J. Antõs and G.P. Yeh, FERMILAB-Conf-99/260.

[22] G. Corcella, E. K. Irish and M. H. Seymour, hep-ph/0012319.

[23] G. Corcella and M. H. Seymour, Phys. Lett. **B442**, 417 (1998).

[24] G. Corcella *et al.*, JHEP **01**, 010 (2000).

[25] G. Corcella, M. L. Mangano and M. H. Seymour, JHEP **07**, 004 (2000).

[26] W. Hollik *et al.*, Nucl. Phys. **B551**, 3 (1999).

[27] B. Grzadkowski and Z. Hioki, Nucl. Phys. **B585**, 3 (2000).

[28] W. Bernreuther, talk given at the ECFA/DESY Linear Collider Workshop, Oxford, UK, March 1999.

[29] M. Beneke *et al.*, hep-ph/0003033, *Proceedings of the Workshop on Standard Model Physics (and more) at the LHC*, CERN 2000-004, p. 419.

[30] R. S. Chivukula, S. B. Selipsky and E. H. Simmons, Phys. Rev. Lett. **69**, 575 (1992), hep-ph/9204214; R. S. Chivukula, E. H. Simmons and J. Terning, Phys. Lett. **B331**, 383 (1994), hep-ph/9404209.

[31] K. Hagiwara and N. Kitazawa, Phys. Rev. **D52**, 5374 (1995), hep-ph/9504332.

[32] U. Mahanta, Phys. Rev. **D55**, 5848 (1997), hep-ph/9611289; Phys. Rev. **D56**, 402 (1997).

[33] J. Jersak, E. Laerman, and P. Zerwas, Phys. Rev. **D25**, 1218 (1982); Yu. L. Dokshitzer, V. A. Khoze, and W. J. Stirling, Nucl. Phys. **B428**, 3 (1994); A. Brandenburg, Eur. Phys. J. **C11**, 127 (1999).

[34] M. Jeżabek and J. H. Kühn, Nucl. Phys. **B314**, 1 (1989); A. Czarnecki, Phys. Lett. **B252**, 467 (1990); C. S. Li *et al.*, Phys. Rev. **D43**, 3759 (1991).

[35] Y. L. Dokshitzer *et al.*, Phys. Lett. **B181**, 157 (1986); L. H. Orr and J. L. Rosner, Phys. Lett. **B246**, 221 (1990), **B248**, 474(E) (1990).

[36] G. Jikia, Phys. Lett. **B257**, 196 (1991); V. A. Khoze *et al.*, Nucl. Phys. **B378**, 413 (1992); Y. L. Dokshitzer *et al.*, Nucl. Phys. **B403**, 65 (1993).

[37] C. Macesanu and L. H. Orr, hep-ph/0012177.

[38] A. Denner *et al.*, Nucl. Phys. **B587**, 67 (2000).

[39] K. Melnikov and O. Yakovlev, Nucl. Phys. B **471**, 90 (1996) [hep-ph/9501358].

[40] W. Beenakker *et al.*, Phys. Lett. **B454**, 129 (1999).

[41] C. Macesanu, in *Physics and Experiments with Future Linear e^+e^- Colliders (LCWS 2000)*, ed. A. Para. (AIP Conference Proceedings, 2001).

[42] W. Beenakker, S. C. van der Marck and W. Hollik, Nucl. Phys. **B365**, 24 (1991).

[43] W. Beenakker *et al.*, hep-ph/9602351.

[44] W. Hollik and C. Schappacher, Nucl. Phys. **B545**, 98 (1999).

[45] A. Denner and T. Sack, Nucl. Phys. **B358**, 46 (1991).

[46] J. Kühn, T. Hahn and R. Harlander, hep-ph/9912262.

[47] C. Macesanu, L.H. Orr, and D. Wackeroth, in progress.